RSC Advances

ROYAL SOCIETY OF CHEMISTRY

www.rsc.org/advances

Journal Name

RSCPublishing

ARTICLE

A nitrogen-doped graphene oxide/cupric oxide as anode material for Lithium ion batteries

Cite this: DOI: 10.1039/x0xx00000x

Received 00th January 2012,
Accepted 00th January 2012

DOI: 10.1039/x0xx00000x

www.rsc.org/

Yue Pan, Ke Ye*, Dianxue Cao, Yiju Li, Yuanyuan Dong, Tengteng Niu, Weijia Zeng, Guiling Wang*

Abstract

A nitrogen-doped graphene oxide/copper oxide (N-GO/CuO) nanocomposite is prepared through modified Hummer method followed by heat treatment. The composite is characterized by scanning electron microscopy and transmission electron microscopy, and the result shows crumpled and curved graphene oxide nanosheets with uniformly distributed CuO nanoparticles. Further study on the composition of N-GO/CuO is identified by fourier transform infrared spectroscopy (FT-IR), Raman spectroscopy, and X-ray photoelectron spectroscopy (XPS). The electrochemical behaviors of N-GO/CuO as anode materials for lithium-ion rechargeable batteries are investigated by galvanostatic discharge/charge measurements and cyclic voltammetry. N-GO/CuO exhibits a high reversible capacity of 472 mAh g^{-1} under the current density of 372 mA g^{-1} with excellent capacity retention of 99.7 % over 100 cycles and improved rate capacities. This work demonstrates N-GO/CuO is a promising anode material for lithium ion batteries.

Key words: Nitrogen-doped; Copper oxide; Modified Hummer method; Anode; Lithium ion battery;

* Corresponding author. Tel./Fax: + 86 451 82589036, *E-mail addresses*: yeke@hrbeu.edu.cn(K. Ye), wangguiling@hrbeu.edu.cn(G. Wang).

Journal Name

RSCPublishing

ARTICLE

1. Introduction

To save or alleviate environmental and energy issue facing to the whole world nowadays, an increasing interest is lithium storage for developing high-performance energy conversion and storage devices [1-3]. The demand for powering high-power vehicles, such as electric vehicles, hybrid electric vehicles and plug-in electric vehicles, cannot be matched well because of the low energy, poor power density and cycling performance, high cost, and long charging time of batteries [4]. In principle, the capability of safe lithium ion batteries (LIBs) depends largely on the performance of electrode materials for lithium storage [5].

Graphite is currently the most common material used for the anodes of commercial batteries because of its capability for reversible lithium intercalation in the layered crystals, which represents the maximum theoretical lithium storage capacity (around 372 mAh g^{-1}). A single layer of graphite, referred to as graphene, has been synthesized using the mechanical exfoliation of graphite by Novoselov et al.[6], and the 2010 Nobel Prize for Physics was awarded to A.Geim and K.Novoselov for this discovery [7]. Graphene have already been exploited for possible energy storage and microelectronics because of its large surface area, good flexibility, good chemical and thermal stability, wide potential windows, especially extraordinary electrical, thermal and mechanical properties [7-9], all of which are advantageous for energy storage and conversion systems. Meanwhile, the graphene decorated with metal oxides or metal salts are attractive within a confined two-dimensional nanostructure interspaces in recent years [9-17], because these composites may not only reduce the stacking degree of graphene but also prevent the volume expansion of metal oxides during cycling process [18]. To improve the specific capacity of graphene and grphene compounds under high charge rates, modification of them with nitrogen has attracted a great deal of attention. This was ascribed to the increased disorder on the surface, enhanced hydrophobicity, and improved electrochemical activity owing to the substitution of nitrogen atoms [19-22].

In general, graphite oxide is synthesized by either the Brodie [23], Staudenmaier[24], or Hummers method [25], or some variation of these methods. Meanwhile, preparation of the dispersions of graphene oxide (GO) made from graphite oxide has appeared. Study about the structure of GO hasn't came to a uniform conclusion. It has been widely assumed that graphene oxide has almost the same layer structure asw graphene, but decorated with hydroxyl and epoxy functional groups between the adjacent layers [26]. The stability of this structure has been studied by Ning liu and Di yin through thermodynamics and kinetics [27], and the hydroxylation of graphene oxide makes it possible to prepare derived composites. The potential performance of GO can be well demonstrate as the composites of GO/polymer and GO/metal oxide have been obtained successfully [28-30].

Herein, we report an approach enabling the fabrications of flexible N-GO/CuO hybrid papers with a low mass loading of CuO. Graphene oxide (GO) as an intermediate during the traditional preparation process of graphene nanosheets (GNs) [25] was prepared from natural graphite. Afterwards, nitrogen-doped graphene oxide/copper oxide nanocomposite was synthesized successfully during the next process. As one of the anode materials for the LIBs, CuO has also been reported [31-36]. The composite of CuO/graphene applied as anode material for LIB and supercapacitor material has been studied [14, 15, 37-39]. However, N-GO or N-GO/CuO as anode material for LIBs has not been studied widely. In this paper, N-GO/CuO as LIB anode significantly enhances the capacity and Li-ion insertion/extraction rate, and a specific capacity of 470 mAh g^{-1} can be achieved under the current density of 372 mA g^{-1} over 100 cycles. More importantly, the electrode shows an excellent stability when the rates decrease from 10 C back to 1 C, with a remaining capacity of 550 mAh g^{-1}, which is almost as high as that under the first 1 C rate. High capacity and excellent electrochemical performance can be achieved for the composite electrode for the energy storage device applications.

2. Experimental

2.1 Preparation of GO

GO was synthesized from spherical natural graphite (Qingdao Furunda Graphite Co., Ltd) by a modified Hummers method, which was reported in previous paper by our group [13].

2.2 Preparation of N-GO/CuO

5 mmol $Cu(NO_3)_2$ and 2.5 mmol NH_4NO_3 were dissolved in 15 mL distilled water to obtain a clear solution, and 10 mL $NH_3 \cdot H_2O$ (30 wt.%) was slowly added subsequently. Blue precipitate of $Cu(OH)_2$ formed initially, then a clear solution was acquired again with the increase of ammonia. A mass of 1 g GO powder was dispersed absolutely into the solution by sonication for 30 min and then the suspension was refluxed at 90 ℃ for 12 h. After that, the composite was obtained by collecting the solid powder, which was dried at 80 ℃ for 10 h in air and calcined at 300 ℃ for 4 h under nitrogen atmosphere. For comparison, N-GO was prepared via the same treating process without adding $Cu(NO_3)_2$.

The morphology was examined by scanning electron microscope (SEM, JEOL JSM-6480) and transmission electron microscopy (TEM, FEI Teccai G2 S-Twin, Philips). The structure was analyzed using X-ray diffraction (XRD, Rigaku TTR III) with Cu Kα radiation (λ=0.1514178 nm). The weight content of CuO in the composite was quantitatively determined by inductively coupled plasma mass spectrometer (ICP-MS, Xseries-II). The component was characterized by Fourier transform infrared spectroscopy (FT-IR, Perkin Elmer SP-100) and X-ray photoelectron spectroscopy with Al Kα radiation (XPS, Thermo ESCALAB 250).

2.3 Electrochemical measurements

Electrochemical experiments were carried out using two-electrode CR2032 coin type half cells. To make working electrodes, slurries of active material (N-GO or N-GO/CuO), carbon black (Ketjenblack EC-600 JD) and poly vinyl difluoride (PVDF) (weight ratio of 85:8:7) in N-methyl-2-pyrrolidone were pasted on pure Cu foil, then the achieved electrode slices were dried under vacuum at 80 ℃ for 12 h and pressed at 10 MPa. A Li foil served as the reference and counter electrode. A concentration of 1.0 mol L^{-1} $LiPF_6$ dissolved in a mixture of ethylene carbonate (EC), dimethyl carbonate (DMC) and ethyl methyl carbonate (EMC) (volume ratio of 1:1:1) was used as the electrolyte. Microporous polypropene film (Celgard 2400) was used as the separator. The cells were finally assembled in a nitrogen-filled glove box. The discharge/charge performance was tested under different current densities (1 C=372 mA g^{-1}) in the potential range of 0.005-3.0 V vs. Li^+/Li on a battery test system (CT-3008-5 V/5 mA, Neware Technology Ltd., Shenzhen, China). Cyclic voltammetry (CV) was conducted using an electrochemical workstation (VMP3/Z, Bio-logic, France).

3. Results and discussion

3.1 Structure and morphology of N-GO/CuO

Fig. 1 shows the XRD patterns of N-GO and N-GO/CuO. There is only a broad peak at 25.1º appeared in the XRD pattern of N-GO, which corresponds to the (002) plane of graphite. This peak occurs at slightly lower angle than that of hexagonal phase graphite (2θ=26.52º，JCPDS card No. 41-1487), indicating that the order structure of graphite was destroyed. Similar XRD patterns were obtained from N-GO/CuO sample. Meanwhile, some small diffraction peaks appear at 2θ of 30~60º, which can be well indexed to CuO (JCPDS card NO. 65-2309). The main diffraction peaks at 35.6º and 38.8º correspond to (111) and (111) planes, respectively. The relative intensity of CuO peaks are not as strong as that of N-GO. The reason should be a low mass concentration and small size of CuO nanoparticles, which will be characterized in the following section.

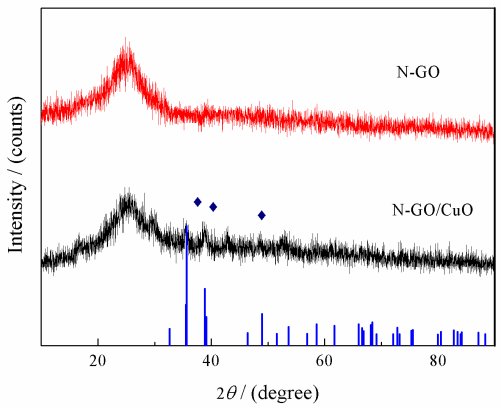

Fig.1. XRD patterns of N-GO and N-GO/CuO

Fig. 2 shows the SEM and TEM images of N-GO and N-GO/CuO. Fig. 2a demonstrates that the interface of obtained N-GO is crumpled and curved with thickness around nano-range. It can be seen that N-GO nanosheets are successfully exfoliated from graphite by the employed process. There is no distinct change appeared on the surface after the decoration process, according to the SEM image of N-GO/CuO shown in Fig. 2b. The TEM images of N-GO and N-GO/CuO are showed in Fig. 2c and 2d, respectively. Fig. 2c displays that N-GO sheets obtained from graphite are supplied with a several-layer structure. CuO presents as nanoparticles with diameter less than 10 nm dispersed within matrix, and the nanoparticles are separated from each other (shown in Fig. 2d). The small size of CuO can be consistent with the result of the XRD (Fig. 1). The small CuO nanoparticles can reduce the stacking degree of N-GO, and the adjacent layers of N-GO can prevent the large volume expansion/contraction and particle aggregation of CuO nanoparticles during the Li^+ insertion and extraction process. Thus, CuO nanoparticles might combine with N-GO sheets tightly during charge/discharge cycling resulting in a high reversible capacity and good cycling stability.

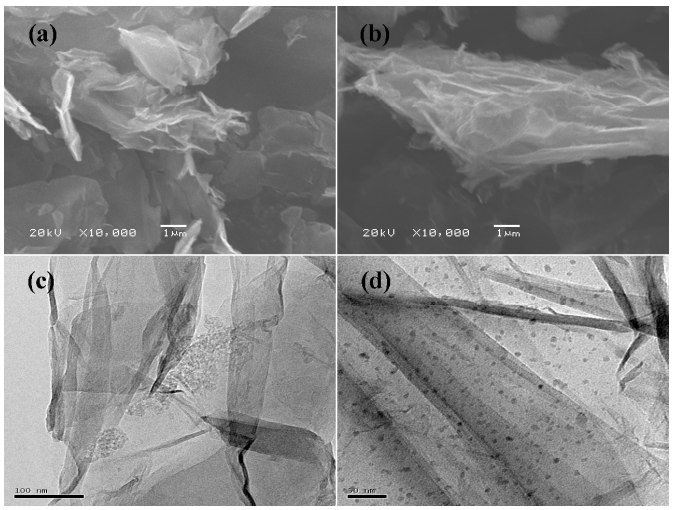

Fig.2. SEM: (a) N-GO (b) N-GO/CuO; TEM: (c) N-GO (d) N-GO/CuO

In order to get detail characterization of N-GO/CuO, Fourier transform infrared spectroscopy was employed. For comparison, Fig. 3 shows the result of characteristic Fourier transform infrared spectroscopy of N-GO and N-GO/CuO, respectively. Both N-GO and N-GO/CuO present the peaks of –CH3 (~2900 cm^{-1}), –CH2 (~2820 cm^{-1}), C-OH (~1230 cm^{-1}), C-N (~1400 cm^{-1}), C=C (~1500 cm^{-1}), C=O (~1750 cm^{-1}) and O-H (~3500 cm^{-1}), which can be well matched with the reported results [45, 46]. And the absorption ~ 500 cm^{-1} of N-GO/CuO could be the characteristic stretching vibrations Cu-O bond in monoclinic CuO [44]. Therefore, the FTIR results show that N-GO/CuO preserves the structure of N-GO and CuO nanoparticles are successfully composited with N-GO.

XPS is employed to reveal the nature of the nitrogen bonds in N-GO/CuO. From the wide-scan XPS spectrums of N-GO/CuO shown in Fig 4a, it is evident to observe that N1s peaks are appeared. The bonding configurations of nitrogen atoms in N-GO/CuO were characterized by high-resolution N1s spectrum. It can be seen from Fig 4b, the N1s peak is resolved into three components, which located at 399.1 eV, 401.1 eV, and 402.7 eV, corresponding to pyridinic, pyrrolic, and graphitic type of N atoms, respectively [45]. It is apparent that pyridinic-N (90.37%) and pyrrolic-N (5.39%) are the two main kinds of N atoms shown in Fig 4b. The pyridinic-N provides a pair of electrons for conjugation with the π-conjugated rings. Thus, it can introduce electron donor properties to N-GO/CuO nanosheets and improve the electrochemical performances. The pyrrolic-N has higher charge mobility due to better electron-donor characteristics and enhanced carbon catalytic activity in electron-transfer reactions, which has significant effects on improving the performance of N-GO/CuO as anode material for LIBs. The mass concentrations (%) and atomic concentrations (%) of C, O, N and Cu in N-GO/ CuO are listed in Table 1.

Table 1. Themass concentrations (%) and atomic concentrations (%) of C, O, N and Cu in N-GO/ CuO

N-GO/ CuO	C	N	O	Cu
Atomic concentration(%)	76.42	5.53	15.98	2.07
Mass concentration (%)	68.88	5.02	16.59	9.51

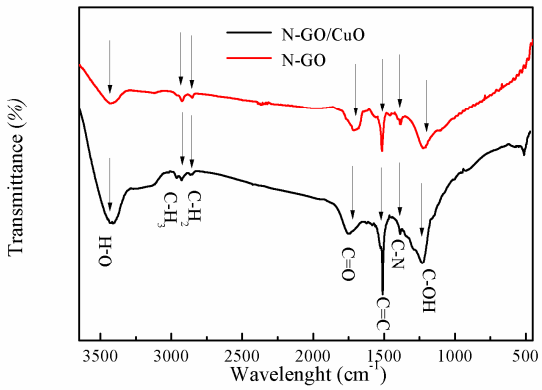

Fig.3. FTIR spectra of N-CuO and N-GO/CuO

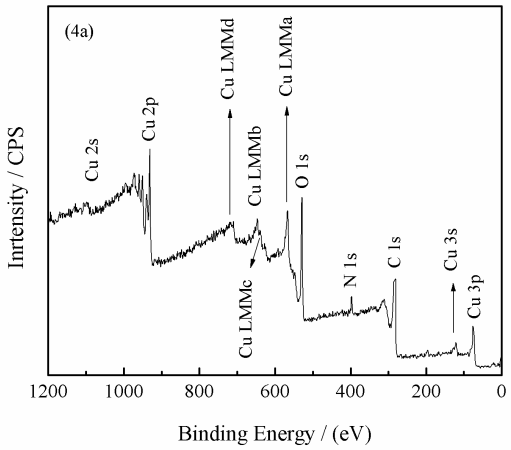

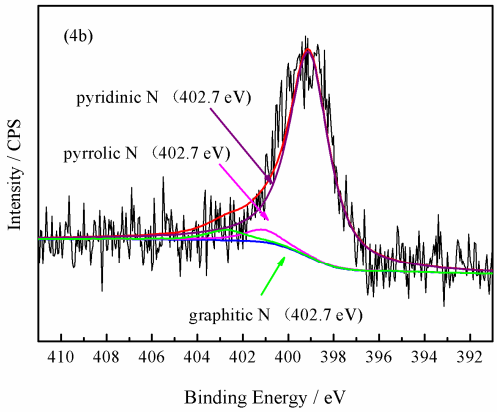

Fig.4. (a) Wide-scan XPS spectrum of N-GO/CuO; (b) High-resolution N1s XPS spectrum of N-GO/CuO

3.2 Electrochemical performance of N-GO/CuO

Galvanostatic discharge/charge experiments were carried out to evaluate the electrochemical performance of N-GO/CuO as anode material for LIB. For comparison, N-GO electrode was also tested under the same conditions. The curves were measured under a current density of 372 mA g^{-1}, in the potential range of 0.05-3 V *vs*. Li^+/Li.

Fig. 5 presents the charge/discharge profiles of N-GO and N-GO/CuO, respectively. Fig. 5a shows the charge/discharge profiles of N-GO electrode in the first three cycles. The first discharge capacity reaches as high as 777.3 mAh g^{-1} with a coulombic efficiency of 87.4 % in the 1st cycle. The specific capacities of the 2nd discharge and charge process are 567.7 and 527.5 mAh g^{-1}, respectively. The values change to 479.8 and 464.2 mAh g^{-1}, with a coulombic efficiency of 96.7 % in the 3rd cycle. While the tendency of the curves shown in Fig. 5b is a little different from that of N-GO. The charge curves suggest a small but obvious curvature change around 2.5 V, which should be contributed to the reduction reaction between CuO nanoparticles and metal lithium. It's worth mentioning that the discharge/charge capacities of N-GO/CuO are 634.2 and 610.6 mAh g^{-1} in the 3rd cycle, corresponding to a coulombic efficiency of 96.3 %. The voltage platforms of CuO are not obvious in the figure, which should be consistent with the low mass ratio in N-GO/CuO according to the characterizations above.

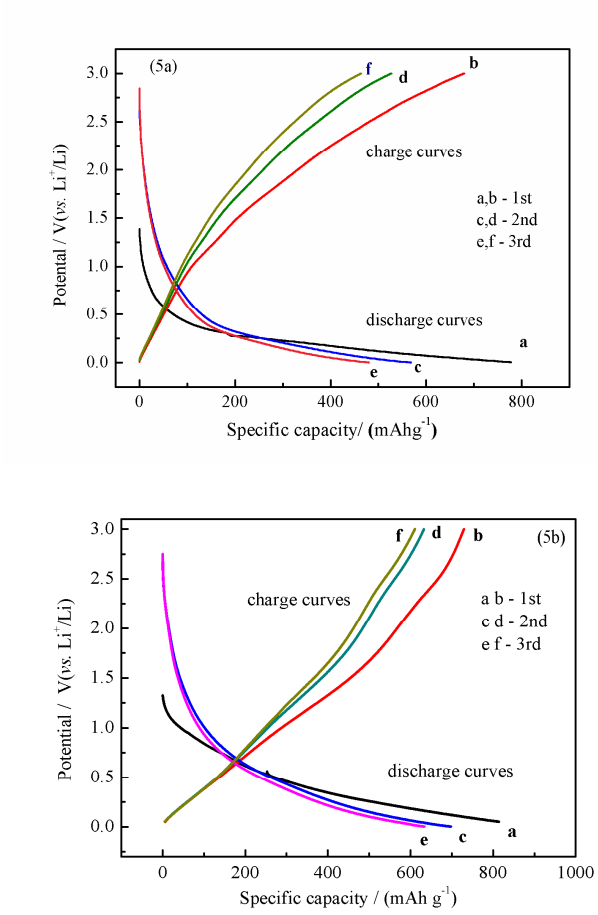

Fig.5. The discharge/charge curves of N-GO (a) and N-GO/CuO (b)

Fig. 6 shows the comparison of cycling performance and stability of N-GO and N-GO/CuO under 1 C, and the coulombic efficiency of N-GO/CuO during the especially stable 20-100 cycles. The initial large irreversible capacities could mainly be caused by the formation of solid electrolyte interface (SEI) and the inactivation of part of Li-ion after cycles and the reaction of Li with C=O, OH, COOH functional group from GO, which occurred primarily in the first cycle. The small loss of capacities in the subsequent cycles can be attributed to the slight pulverization and aggregation of active material, which lead to the reduction between active material and current collector. The capacities of N-GO in the first two cycles were close to these of N-GO/CuO, but the values decayed fast in the following 40 cycles. The value of discharge capacity decreased to306.2 mAh g^{-1} after 100 cycles with 76.7 % retention of the stable reversible capacity compared with that in the 20th cycle. In contrast, N-GO/CuO presents a higher electrochemical reversibility and stability. After 100 cycles, N-GO/CuO obtains a high discharge capacity of 472 mAh g^{-1}. The capacity retention is 98.1 %, corresponding to the value of 479 mAh g^{-1} in the stable 20th cycle. The higher reversible capacity achieved after the process of decoration of raw GO should be attributed to the addition of CuO and nitrogen, the subdued aggregation between the adjacent layers of N-GO/CuO and the interfacial storage mechanism in which an excess lithium is accommodated in these boundary regions via charge separation between nanoparticles and Li_2O grains until the lithium potential approaches the value of pure Li [47, 48]. Meanwhile, the values of the coulombic efficiencies of N-GO/CuO during the stable 20th ~ 100th cycles are almost larger than 99.5 %. The results demonstrate the possibility of N-GO/CuO as anode for LIBs.

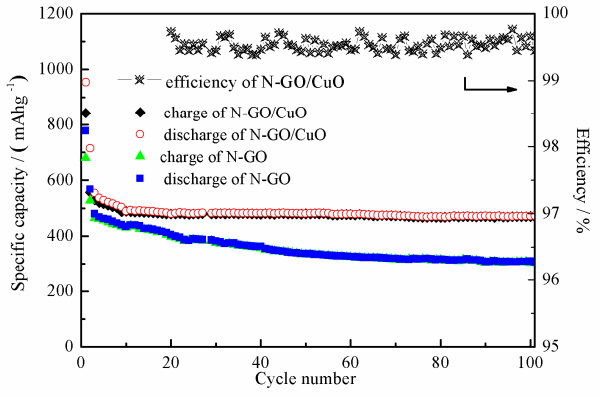

Fig.6. Cycling performances under 1 C for N-GO, N-GO/CuO, and the coulombic efficiency of N-GO/CuO

For a further application, good rate capability is necessary for the electrode materials. The observed high and stable specific

capacities of N-GO/CuO encourage the study of rate capabilities using various current densities at ambient temperature. The discharge/charge capacities under different 5 current densities in the range from 1-10 C (1C=372 mA g^{-1}) are given in Fig. 7. The currents were changed in 6 steps after every 4 cycles. After the current density was increased gradually to 10 C, it was decreased abruptly to 1 C. Under the high current rate of 10 C (3720 mA g^{-1}), the reversible capacity of N-GO/CuO was maintained as high as 350 mAh g^{-1}. The results are highly attractive, compared with other high-performance nanostructured anode materials. When the current rate was decreased from 10 C to 1 C, the capacity increased to 550 mAh·g^{-1}, which is almost as high as the first 1 C rate. In addition, the coulombic efficiency variations under different current densities were illustrated in Fig. 6. The values were all around 100 %, except the first discharge/charge process. Both the high reversible capacity and the good rate performance are benefited from the special structure and improved electrical conductivity of N-GO/CuO. The results indicate improved C-rates performance of N-GO/CuO.

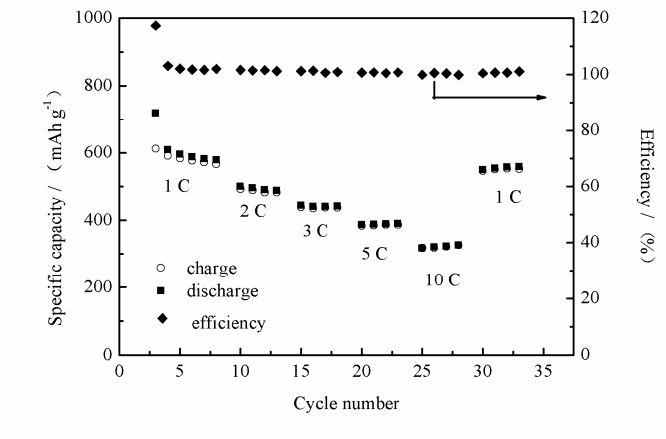

Fig.7. Cycling stability at various C rates of N-GO/CuO

The CuO/graphene nanocomposite electrodes for LIB reported by Seung-Deok Seo [14] has a weight ratio of CuO:GNS (82:18 wt%). The specific capacity under the current density of 120 mA g^{-1} could reach 800 mAh g^{-1} at the 3rd cycle and the value decreased to 500 mAh g^{-1} at the 30th cycle with a serious capacity lost. The CuO/graphene composite reported by Y.J. Mai [15] has a weight ratio of CuO:GNS (88:12 wt%). The CuO/graphene composite exhibited a reversible capacity of 561.4 mAh g^{-1} under the current density of 67 mA g^{-1}. After 50 cycles the discharge capacity remained 423 mAh g^{-1} with 75.3% retention of the reversible capacity. According to the results of cycling performance (Fig.5) and rate performance (Fig.6), N-GO/CuO in this work has better performance, especially the cycling stability than previous literatures.

The good electrochemical performance of N-GO/CuO should be due to the synergic effect between CuO nanoparticles and N-GO nanosheets. High specific surface area, appropriate pore size, and surface functional groups (C=O, C-O, C-O-C, which were approved in the result of FTIR) can been considered as the effective ways to improve the specific capacities of N-GO/CuO. It is believed that surface functional groups can help the adsorption of lithium ions and then improve the tability and facilitated rapid lithium ion transport within the nanosheet. Then, the special functional groups in the structure of N-GO/CuO can prevent CuO particles from agglomerating and contribute to the high dispersion of CuO nanoparticles on the surface of the nanosheet at the same time [49]. By this way, these functional groups can improve the performances of N-GO/CuO. The high dispersion of CuO nanoparticles can reduce the stacking degree of N-GO as backbone among the thin nanosheets, and also prevent the agglomeration of adjacent metal oxide nanoparticles during cycling process.

For a further understanding of the mechanism of N-GO/CuO as anode material for LIB, cyclic voltammetry (CV) was investigated. Fig. 8 shows the results of CV analysis of N-GO and N-GO/CuO, respectively. The tests were performed in the voltage window of 3.0-0.05 V at a scan rate of 0.1 mV S^{-1}. The peaks below 0.2 V for the electrodes manifest that the reversible Li intercalate graphene oxide to form LiC_6, which is similar to that of graphene [46]. N-GO/CuO shows a characteristic peak at ~ 2.5 V which is related to the process $2Cu + Li_2O \rightarrow Cu_2O + 2Li$ [33]. This peak is in good correspondence with the plateau observed at the same potential in the discharge/ charge profiles (Fig. 4b). The mechanism of CuO as anode for LIB can be described as:

$CuO + 2Li \Leftrightarrow Cu + Li_2O$ (theoretical value is 675mAh g^{-1})

A. Débart [50] has reported that the reduction mechanism of CuO by lithium involved the formation of a solid solution of $Cu^{II}_{1-x} + Cu^{I}_{1-x}O_{1-x/2}$ ($0 \leq x \leq 0.4$), a phase transition into Cu_2O, then the formation of Cu nanograins dispersed into a lithia matrix (Li_2O) followed by the growth of an organic-type coating. During the subsequent charge, the organic layer vanished first, and then the Cu grains were partially or fully oxidized with a concomitant decomposition of Li_2O.

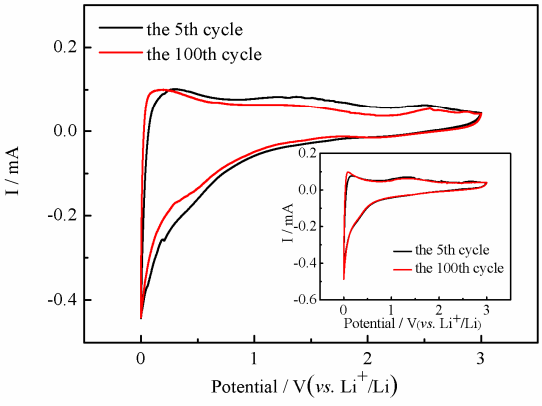

Fig.8. CV curves of N-GO/CuO and GO in the 5th and 100th cycles

In the anode curve, the little and weak peaks at 0.2 V can be attributed to Li deintercalation from LiC_6 [51]. EunJoo Yoo [8] has reported explicitly reversible lithium storage in graphene. Previously, a lot of studies have been undertaken to elucidate the lithium intercalation mechanism into graphite [52-56]. It is accepted that lithium occupies the sites between two adjacent graphene planes, and each lithium within a plane is associated with a hexagonal C ring in such a way as to avoid the nearest neighbor occupation. In case of the graphene structure, the storage sites might be more readily accessible as compared to graphite. The fact that lithium adsorption can take place on two sides of the graphene layer and multilayer adsorption [57] at a high chemical potential of lithium, which can give rise to higher Li storage capacities. According to the similar layer structure between graphene and N-GO, N-GO should have similar mechanisms and remarkably potential application in lithium storage. In addition, the peak intensity difference between 5th and 100th cycle is very small, which indicate the high capacity reversibility during the cycles. It is also easy to find that N-GO play a more important role in the capacities according to the curves (Fig. 5a and Fig. 5b).

Electrochemical impedance spectroscope (EIS) was applied to interpret the change of electrochemical performance by applying a sine wave with amplitude of 5.0 mV in the frequency range of 10 mHz – 100 kHz. Fig. 9a displays the typical Nyquist plots of freshly assembled cells of N-GO and N-GO/CuO, respectively. The semicircle in the high-frequency range can be caused by the charge transfer process on the surface between the electrolyte and electrode or metallic lithium counter electrode. The straight line in the low-frequency range is due to the lithium-ion diffusion and accumulation process in the working electrodes. It can be seen from Fig. 9a that the semicircles are about 56 Ω and 43 Ω in terms of the total charge transfer resistance of the fresh cells of N-GO and N-GO/CuO, respectively. This result manifests that the doped nitrogen can reduce the resistance and improve the electrochemical performances. Fig. 9b shows typical Nyquist plots of the freshly assembled cell of N-GO/CuO and the same cell after 50 discharge/charge cycles. The semicircle becomes smaller and the resistance value decreases to about 15 Ω after 50 cycles, suggesting an easier reaction process after several cycles. This decrease of the resistance may correspond to the wetting process between electrode and liquid electrolyte. The electrode could then possess a higher reactivity and lower polarization. On the other hand, the changes in impedance are also associated with the component modifications of the electrode.

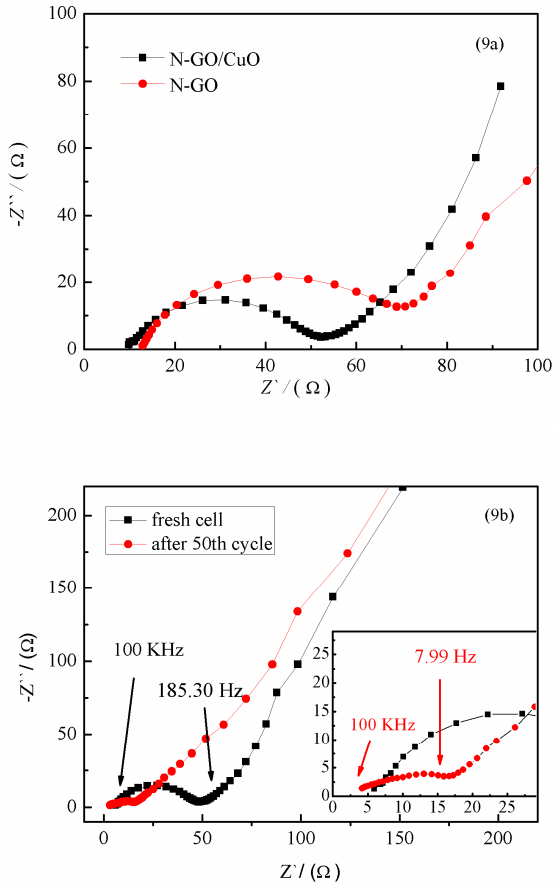

Fig.9. Electrochemical impedance results on fresh N-GO and N-GO/CuO electrodes (a) and those obtained before the 1st cycle and after the 50th cycle of N-GO/CuO electrode (b).

Conclusions

In summary, N-GO/CuO was synthesized successfully through modified Hummer method. Results showed that the small size of the CuO nanoparticles were uniformly distributed among the layers of N-GO. The discharge capacities of N-GO/CuO electrode were 480.3 and 472.6 mAh g^{-1} in the 20th and 100th cycles under the current density of 372 mA g^{-1}, respectively. The high capacities benefit from the terrific electrical conductivity, large effective surface area of N-GO/CuO and the addition of CuO nannoparticles, which played an important role in supporting the layer structure of GO and avoiding agglomerate. Good rate capability is also another impact on the promising application of N-GO/CuO.

Acknowledgements

We gratefully acknowledge the financial support of this research by the National Natural Science Foundation of China (21403044), the Heilongjiang Postdoctoral Fund (LBH-Z13059), the China Postdoctoral Science Foundation (2014M561332) and the Fundamental Research Funds for the Central Universities (HEUCF201403018).

References

1 Z. Chen, M. Zhou, Y. Cao, X. Ai, H. Yang, J. Liu, *Adv. Eng. Mater*. 2012, **2**, 94.
2 V. Etacheri, R. Marom, R. Elazari, G. Salitra, D. Aurbach, *Energy Environ. Sci.*, 2011, **4**, 3243.
3 L. Ji, Z. Lin, M. Alcoutlabi, X. Zhang, *Energy Environ. Sci.*, 2011, **4**, 268.
4 I.T. Kim, A. Magasinski, K. Jacob, G. Yushin, R. Tannenbaum, Tannenbaum, *Carbon*, 2013, **52**, 56.
5 A. Manthiram, Materials Challenges and Opportunities of Lithium Ion Batteries, *J. Phys. Chem. Lett.* 2011, **2**, 176.
6 D. Guerard, A. Herold, Intercalation of lithium into graphite and other carbons, *Carbon*, 1975, **13**, 337.
7 K.S. Novoselov, A.K. Geim, S.V. Morozov, D. Jiang, Y. Zhang, S.V. Dubonos, I.V. Grigorieva, A.A. Firsov, *Science*, 2004, **306**, 666.
8 E. Yoo, J. Kim, E. Hosono, H. Zhou, T. Kudo, I. Honma, *Nano Lett.* 2008, **8**, 2277.
9 Z.-S. Wu, G. Zhou, L.-C. Yin, W. Ren, F. Li, H.-M. Cheng, *Nano Energy* 2012, **1**, 107.
10 T. Hu, X. Sun, H.T. Sun, M.P. Yu, F.Y. Lu, C.S. Liu, J. Lian, *Carbon,* 2013, **51**, 322.
11 H.B. Zhao, L.Y. Pan, S.Y. Xing, J. Luo, J.Q. Xu,, *J. Power Sources,* 2013, **222**, 21.
12 H. Xia, D.D. Zhu, Y.S. Fu, X. Wang, *Electrochim. Acta*, 2012, **83**, 166.
13 G.L. Wang, J.C. Liu, S. Tang, H.Y. Li, D.X. Cao, *J. Solid State Electrochem.*, 2011, **15**, 2587.
14 [B. Zhao, H. Zhuang, T. Fang, Z. Jiao, R.Z. Liu, X.T. Ling, B. Lu, Y. Jiang, *J. Alloys Comp.* 2014, **597**, 291.
15 Y.J. Mai, X.L. Wang, J.Y. Xiang, Y.Q. Qiao, D. Zhang, C.D. Gu, J.P. Tu, *Electrochim. Acta,* 2011, **56**, 2306.
16 Z.S. Wu, W.C. Ren, L. Wen, L.B. Gao, J.P. Zhao, Z.P. Chen, G.M. Zhou, F. Li, H.M. Cheng, *ACS Nano*, 2010, **4**, 3187.
17 A.K. Rai, T.V. Thi, J. Gim, J. Kim, *Mater. Charact.* 2014, **95**, 259
18 B.-d. Chen, C.-x. Peng, Z. Cui, *Trans. Nonferrous Met. Soc. China* 2012, **22**, 2517.
19 J. Wang, L. Shen, H. Li, X. Wang, P. Nie, B. Ding, G. Xu, H. Dou, X. Zhang, *Electrochim. Acta*, 2014, **133**, 209.
20 T. Hu, M. Xie, J. Zhong, H.-t. Sun, X. Sun, S. Scott, S. M. George, C.-s. Liu, J. Lian, *Carbon*, 2014, **76**, 141.
21 L. Chen, Y. Zhang, C. Lin, W. Yang, Y. Meng, Y. Guo, M. Li, D. Xiao, *J. Mater. Chem. A*, 2014 (2), 9684.
22 J.-P. Jegal, K.-C. Kim, M.S. Kim, K.-B. Kim, *J. Mater. Chem. A* 2014, **2**, 9594.
23 B.C. Brodie, *Philos. Trans. R. Soc. London* 1859, **149**, 249.
24 L. Staudenmaier, Ber. Dtsch, *Chem. Ges.* 1898, **31**, 1481.
25 W.S. Hummers, R.E. Offeman, Preparation of Graphitic Oxide, *J. Am. Chem. Soc.* 1958, **80**, 1339.
26 H.-M. Ju, S.H. Huh, S.-H. Choi, H.-L. Lee, *Mater. Lett.* 2010, **64**,. 357.
27 N. Lu, D. Yin, Z. Li, J. Yang, Structure of Graphene Oxide: Thermodynamics versus Kinetics, *J. Phys. Chem. C*, 2011, **115,** 11991.
28 A.S. Patole, S.P. Patole, S.-Y. Jung, J.-B. Yoo, J.-H. An, T.-H. Kim, *Eur. Polym. J.*, 2012, **48**, 252.
29 Y. Lin, J. Jin, M. Song, *J. Mater. Chem*. 2011, **21**, 3455.
30 V.K. Singh, M.K. Patra, M. Manoth, G.S. Gowd, S.R. Vadera, N. Kumar, *New Carbon Mater*, 2009, **24**, 147.
31 C.S. Choi, Y.U. Park, H. Kim, N.R. Kim, K. Kang, H.M. Lee, *Electrochim. Acta*, 2012, **70**, 98.
32 X.H. Huang, C.B. Wang, S.Y. Zhang, F. Zhou, *Electrochim. Acta*, 2011, **56**, 6752.
33 J.Y. Xiang, J.P. Tu, L. Zhang, Y. Zhou, X.L. Wang, S.J. Shi, *Electrochim. Acta,* 2010, **55**, 1820.
34 L.L. Wang, H.X. Gong, C.H. Wang, D.K. Wang, K.B. Tang, Y.T. Qian, *Nanoscale*, 2012, **4**, 6850.
35 C. Wang, Q. Li, F.F. Wang, G.F. Xia, R.Q. Liu, D.Y. Li, N. Li, J.S. Spendelow, G. Wu, *ACS Appl. Mater. Interfaces*, 2014, **6**, 1243.
36 J. Wang, Y.C. Liu, S.Y. Wang, X.T. Guo, Y.P. Liu, *J. Mater. Chem. A* 2014, **2**, 1224.
37 A. Pendashteh, M. F. Mousavi, *Electrochim. Acta*, 2013, **88**, 347.
38 A.K. Rai, L.T. Anh, J. Gim, V. Mathew, *J. Power Sources*, 2013, **244**, 435.
39 Y. Liu, W. Wang, L. Gu, Y.W. Wang, Y.L. Ying, Y.Y. Mao, L.W. Sun, X.S. Peng, *ACS Appl. Mater. Interfaces*, 2013, **5**, 9850.
40 J.W. Lee, A.S. Hall, J.-D. Kim, T.E. Mallouk , *Chem.Mater.* 2012, **24**, 1158.
41 Y. Fang , Bin Luo, Y.Y. Jia, X.L. Li, B.Wang, Q. Song, F.Y. Kang, L.J. Zhi, *Adv. Mater.*, 2012, **24**, 6348.
42 D.Q. Gao, G.J. Yang , J.Y. Li, J. Zhang, J.L. Zhang, D.S. Xue, *J. Phys. Chem. C*, 2010, **114**, 18347.
43 M. Dar, S. Nam, Y. Kim, W. Kim, *J. Solid State Electr.* 2010, **14**,1719.
44 Y.Y. Xu, D.R. Chen, X.L. Jiao, *J. Phys. Chem. B*, 2005, 109, 13561.
45 Y.J. Li, K. Ye, K. Cheng, D.X. Cao, Y. Pan, S.Y. Kong, X. Zhang, G.L. Wang, , *Journal of Electroanalytical Chemistry*, 2014, **727**, 154.
46 H.D. Liu, J.M. Huang, X.L. Li, J. Liu, Y.X. Zhang, K. Du, *Appl. Surf. Sci*. 2012, **258**, 4917.
47 P. Balaya, H. Li, L. Kienle, J. Maier, *Adv. Funct. Mater.* 2003, **13**, 621.
48 J. Maier, *Angewandte Chemie International Edition*, 2013, **52**, 4998.
49 Y.-T. Kim, K. Tadai, T. Mitani, *J. Mater. Chem.*. 2005, **15**, 4914.
50 A. Debart, L. Dupont, P. Poizot, J.B. Leriche, J.M. Tarascon, *J. Electrochem. Soc.* 2001, **148**, A1266.
51 X. Wang, X. Zhou, K. Yao, J. Zhang, Z. Liu, *Carbon,* 2011, **49**, 133.

52 D. Guerard, A. Herold, *Carbon*, 1975, **13**, 337.
53 M. Zanini, S. Basu, J.E. Fischer, *Carbon*, 1978, **16**, 211.
54 N. Kambe, M.S. Dresselhaus, G. Dresselhaus, S. Basu, A.R. McGhie, J.E. Fischer, *Materials Science and Engineering*, 1979, **4**0, 1.
55 J. R. Dahn, *Physical Review B*, 1991, **44**, 9170.
56 T. Ohzuku, Y. Iwakoshi, K. Sawai, *J. Electrochem. Soc.* 1993, **140**, 2490.
57 M. Deschamps, R. Yazami, *J. Power Sources*, 1997, **68**, 236.